Using computer graphics and film technologies, engineers can now numerically model the nondestructive testing technique that detects flaws in the pressurized steam pipes of nuclear power plants.

Simulating Electromagnetic NDT Probe Fields

Nathan Ida and William Lord
Colorado State University

If a defect exists in a critical system component—particularly in an aerospace, power, or transportation system—lives can depend on its early detection. Electromagnetic methods of nondestructive testing (NDT) are widely used to search out these defects by measuring the interaction of excitation fields with flaws in the part under test.

When the part under test happens to be the Inconel tubing in pressurized nuclear reactor steam generators (the domain of this article), then the concern for operational safety and reliability is particularly acute. Inconel tubing is used where the heat from the reactor coolant converts water into steam for the generation of electrical power.

Since regulatory agencies require that Inconel tubing be periodically tested with an eddy current probe and because electromagnetic field/defect interactions are particularly difficult to model analytically, we felt it would be useful to investigate a numerical approach to steam generator tubing inspection—an approach that makes use of both computer graphics and film technologies.

Figure 1 shows details of a steam generator's construction along with a typical eddy current probe and associated instrumentation. The probe itself consists of two coils wound differentially and excited with an alternating current that runs from 100 to 500 kHz. In a clean tube, both coils are exposed to identical conditions, and the output of the probe's bridge circuit, calibrated to provide a Cartesian plot of the real and imaginary parts of the probe impedance, is zero. As the probe passes a tube defect or some other anomaly, the probe's balance is disturbed and an "impedance plane trajectory" is produced. A typical calibration support plate signal for a differentially connected eddy current probe is shown in Figure 2.

Traditionally, eddy current nondestructive testing phenomena have been modeled analytically, and the relevant descriptive partial differential equations have been solved by classical techniques after appropriate assumptions have been made with regard to material nonlinearities and geometrical constraints.[1] To date, the analytical modeling approach has only been applied to the simplest of geometries and shows no promise of providing the flexibility needed to solve the general defect characterization or inverse problem.

As we performed the work described in this article, one of our major objectives was to determine whether or not finite element analysis (a numerical rather than analytical technique that was originally developed for the study of magnetic fields in electrical machinery[2-4]) could be applied to the study of eddy current NDT phenomena, particularly as they relate to the inspection of steam generator tubing. We felt that such a model was needed to

(1) describe the physics of interaction between the applied AC field, induced eddy currents, and defects in the test specimen;

(2) serve as a theoretical testbed for situations that are difficult or impossible to replicate experimentally;

(3) generate eddy current output signals for a wide variety of defect and specimen shapes (avoiding costly sample preparation), thus aiding in the determination of defect characterization parameters; and

(4) help in the design of eddy current probes for specific applications.

0272-1716/83/0500-0021$01.00 © 1983 IEEE

The finite element solution

Since the geometry encountered in nondestructive testing of steam generator tubing and its support plate is cylindrical, an axisymmetric formulation was chosen for the analysis. A sinusoidal current source with a density of $\mathbf{j}_s[\mathbf{a}/m^2]$ is applied to a circular coil, and the magnetic vector potential is found everywhere in the region of interest by solving a Poisson type of diffusion equation[5]

$$\frac{\partial^2 \mathbf{a}}{\partial R^2} + \frac{1}{r}\frac{\partial \mathbf{a}}{\partial r} + \frac{\partial^2 \mathbf{a}}{\partial z^2} - \frac{\mathbf{a}}{r^2} = -\mu \mathbf{j}_s + j\omega\sigma\mu\mathbf{a} \quad (1)$$

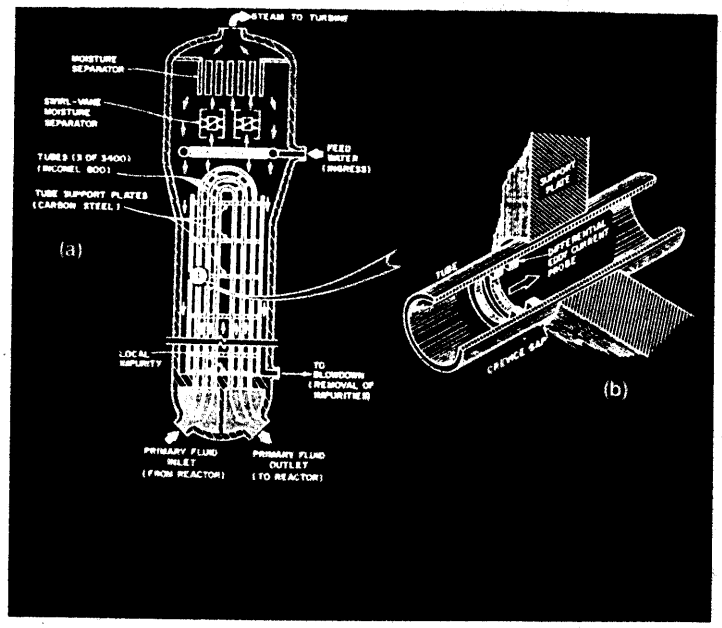

Figure 1. Eddy current testing of steam generator tubing: details of generator construction (a); eddy current probe and instrumentation (b).

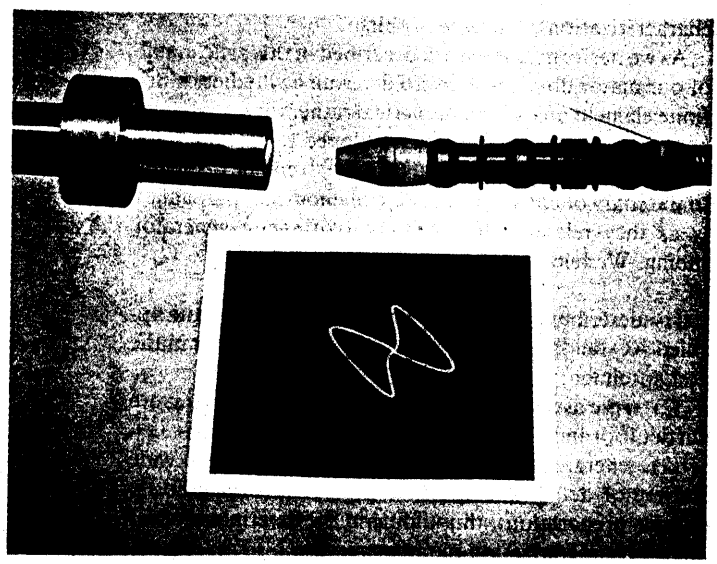

Figure 2. Typical impedance plane trajectory for a differential eddy current probe.

where μ is the magnetic permeability, ω is the angular frequency, σ is the electrical conductivity, and j is the complex operator. The eddy current density induced by the source is

$$\mathbf{j}_e = -j\omega\sigma\mathbf{a} \quad (2)$$

Instead of solving equation 1 directly, we applied a variational principle that results in an energy-related functional, which upon minimization yields a correct solution to equation 1[6]:

$$F = \int \left[\int \frac{1}{\mu}\,\mathbf{b}\,d\mathbf{b} + \frac{1}{2} j\sigma\omega\,|\mathbf{a}|^2 - \mathbf{j}_s\cdot\mathbf{a} \right] dv \quad (3)$$

where $\mathbf{b}$ is the flux density.

To solve for $\mathbf{a}$, we discretized the region of interest into a large number of finite elements. In this case, first-order (linear) triangular elements are used (see Figure 3). Each element is a volume of space with a triangular area in the x-z plane and a "depth" of $2\pi r_c$, where r_c is the normal distance of the centroid of the element from the z axis. The magnetic vector potential has discrete values at each of the three element nodes, and a set of linear interpolating functions is used to describe the magnetic vector potential within the element.

The magnetic flux density is found from $\mathbf{b} = \nabla \times \mathbf{a}$ and is therefore constant within the element. The linear variation of $\mathbf{a}$ within each element is significant—significant not only for finite element formulation, but also for graphic display because two points of equal $\mathbf{a}$ on two edges of an element are connected by a straight line. (This is later used in plotting the field distribution around the eddy current coils.)

Using the interpolation functions, we perform the volume integration in equation 3 over the volume of each element, and then minimize the total functional by setting its partial derivative with respect to the unknown value of $\mathbf{a}$ at each node in the solution region to zero. This results in a system of linear equations that is solved for $\mathbf{a}$ by Gaussian elimination:

$$[\mathbf{G}]\{\mathbf{a}\} = \{\mathbf{q}\} \quad (4)$$

where $[\mathbf{G}]$ is an $n \times n$ banded symmetric complex matrix, $\{\mathbf{q}\}$ is an $n \times 1$ complex source vector, and $\{\mathbf{a}\}$ is an $n \times 1$ complex unknown vector. For all of these, n is the total number of nodes in the solution domain. Numerical values of $\mathbf{a}$ are obtained for each node of the region and are later used for the calculation of the flux densities and the impedance of the source coils.[7]

As we stated earlier, the eddy current probe used in the analysis consists of two differentially connected coils. The complex impedance ($\mathbf{z}$) of this arrangement can be calculated from the magnetic vector potential ($\mathbf{a}_c$) at the centroid of each triangle that forms the probe cross section (Figure 3):

$$\mathbf{z} = \frac{j\omega 2\pi \mathbf{i}_s}{\mathbf{i}_s^2}\left[\sum_{j=1}^{N_b} (r_{cj} \triangle j)\mathbf{a}_{cj} - \sum_{j=1}^{N_a} (r_{cj} \triangle j)\mathbf{a}_{cj} \right] \quad (5)$$

where $\mathbf{i}_s$ is the current source, r_{cj} is the centroidal distance of the jth triangular element, and N_a and N_b are the number of elements forming coils a and b, respectively.

The situation described above is summarized in Figure 3, where only half of the region is discretized due to the

symmetry about the z axis. The solution results in a specific flux distribution over the entire region and returns a single impedance value for the probe.

If the coil is moved to a different location, a different flux distribution will result, changing the value of the probe impedance. By moving the coil in small increments (about 0.040 inch each), we obtained a series of flux distribution plots along with the corresponding values of the probe impedance. When plotted, these values result in a closed curve (the impedance plane trajectory) that is characteristic of the support plate's properties and condition.

For purposes of illustration, the impedance plane trajectory for the support plate described in this article is a predicted trajectory because of the dramatic changes that always occur in the probe field at the entrance to the tube hole.

Computer programs and results

The finite element solution described above was carried out on a Cyber 720 computer. A total of 70 probe positions were examined separately—positions that reflected both probe movement and flux distribution up to the point where the probe was aligned in the center of the support plate.

The finite element discretization was produced by an automatic mesh generator that divided the region into a total of 6000 triangular elements with 3146 nodes. This mesh either has to be generated for each probe position or modified in some other way to reflect the new position of the coils. We opted for the latter alternative as it was more economical in the case at hand.

The finite element solution for each probe position consists of the numerical integration of the energy functional (equation 3) assembly of the global matrix and its solution by means of Gaussian elimination and back substitution; this yields the unknown values of $\mathbf{a}$ at each node of the mesh. Unlike the mesh generation, the finite element solution must be carried out for each probe position. The matrix, as mentioned in the previous section, is banded and symmetric and has a semibandwidth of 27, thus resulting in a 3146×27 matrix that must be inverted.

For each probe position, an output file was created with the values of the magnetic vector potential $\mathbf{a}$ and probe impedance $\mathbf{z}$, and the data was transferred to a Tektronix 4081 graphics system for processing and plotting.

On-line graphic display of the output from the finite element program, although desirable, was ruled out as both meaningless and too expensive. It takes about 30 seconds of CPU time for the finite element program (excluding data generation) to be completed for each frame

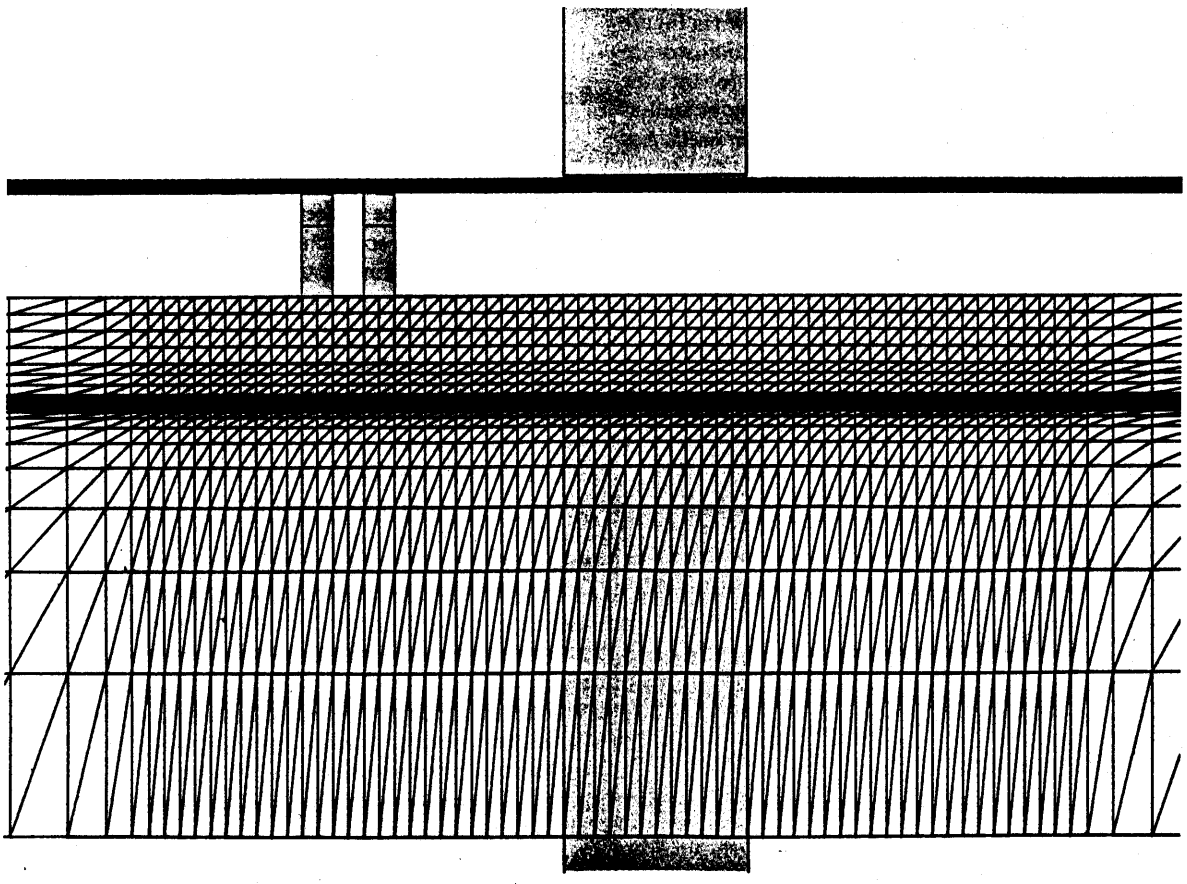

Figure 3. Finite element discretization of the region around the support plate.

(probe position). The program had to be run as a batch job due to its size, memory requirements, and the large size of both input and output files. Also, the output has to be processed before display, and filming the animation frame off the screen proved impractical for reasons that will be explained shortly.

The graphics system

The Tektronix 4081 graphics system that was used to produce the probe animation sequence is shown in block diagram form in Figure 4. The Tektronix display, even though it was large and clear, could not be used for direct off-the-screen filming for the following reasons:

(1) The low intensity and relatively high background noise of the picture tube resulted in poor quality photographs.

(2) The curvature of the screen was quite apparent in test photographs.

(3) The starting point for each plot on the screen is not the same. This is not apparent when viewing only a few frames, but in a test sequence taken off the screen, we noticed that the frames were moving in a small, but noticeable, semicircular pattern. This phenomenon is peculiar to the screen and does not happen when the frames are plotted on the plotter.

(4) Color was considered important for overall picture clarity, and could be introduced into the image only by plotting the output on a Tektronix 4663 digital plotter.

The Tektronix 4905 mass storage unit, shown in Figure 4, consists of a dual hard disk unit with a total storage capability of 10M bytes. This unit was used to store the output files from the finite element program as well as the plot files generated on the graphics system itself. Additionally, a telephone line connection to the Cyber 720 allows the system to be used for data transfer to and from the Cyber or to function as a peripheral unit.

The plotting routines were written in Fortran IV with some special statements added for data display on the 4081. Each frame could be displayed on the screen by a single routine, but on the plotter, three different programs were used for convenience: one for plotting the flux lines and coils; one for plotting the impedance trajectories; and a third for plotting the support plate and tube. This arrangement let us use more colors in a frame than the plotter's two programmable colors.

Since the output from the finite element solution consists of the magnetic vector potential at the nodes of the mesh only, for contour plotting we used a linear extrapolation technique to calculate the vector potential value at any point along the edges between any two nodes. The same technique could be used to calculate additional values inside the element, but we considered this unnecessary because of the large number of elements and their small size. Therefore, the contour lines are composed of straight segments, each running across one element. The result, however, is very smooth, as can be seen in Figures 5-9.

As mentioned earlier, 70 frames were generated by the finite element program, describing the probe's movement up to the middle of the support plate. In the film produced from the plotter's output, however, the probe was moved past the support plate. The necessary extra frames were generated by reflecting frames 1 to 70 at the middle of the support plate for both the flux line plots and impedance trajectory plots. This could be done because of the symmetry of the arrangement. Thus, for example, the plots in Figures 6 and 8 were generated from the same finite element output.

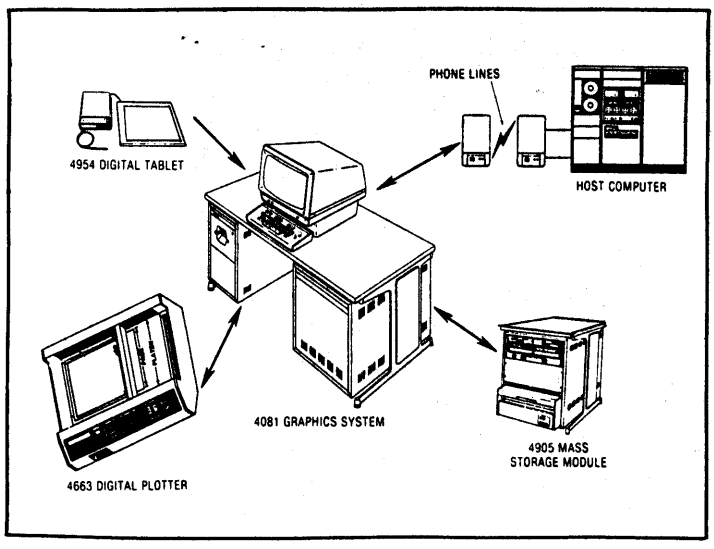

Figure 4. The Tektronix 4081 graphics system.

The animation sequence

After proper scaling and positioning relative to each other, the three different parts of each frame—the flux line plot, impedance trajectory, and support plate and tube—were plotted for each of the 139 frames of the animation sequence. However, the first and last few frames carry very little information in terms of flux and impedance changes, so these were left out of the film. As a result, a total of 131 frames were filmed, each one being shot twice. (The duplication of frames is a standard animation technique.) Figures 5-9 represent a sequence of five frames from the animation sequence.

In Figure 5, the coils are both well away from the support plate, thus both have essentially the same field distribution. The single point to the left represents the impedance of the probe at this particular probe position.

In Figure 6, the leading coil is close to the edge of the support plate, and a dramatic change in the flux distribution has taken place compared to Figure 5; however, the trailing coil has a distribution that has changed very little. The change in the impedance is clearly noticeable. It should be remembered, though, that there are some 35 frames between those shown in Figures 5 and 6.

Figure 7 represents the situation where the coils are aligned in the middle of the support plate. Since the two coils are differentially connected, this situation is identical to the one in Figure 5 in terms of impedance, and the impedance trajectory has now described a closed loop.

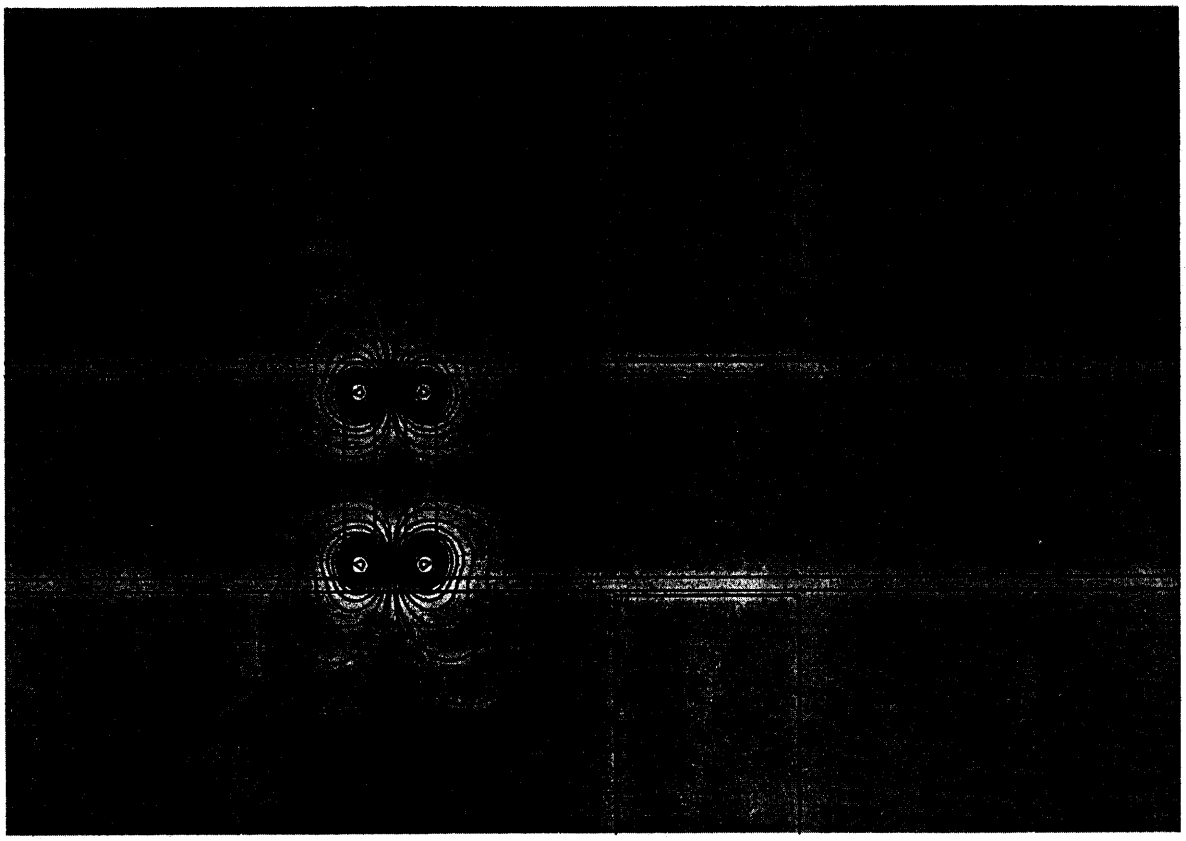

Figure 5. Magnetic field line contour plot with coils far from support plate.

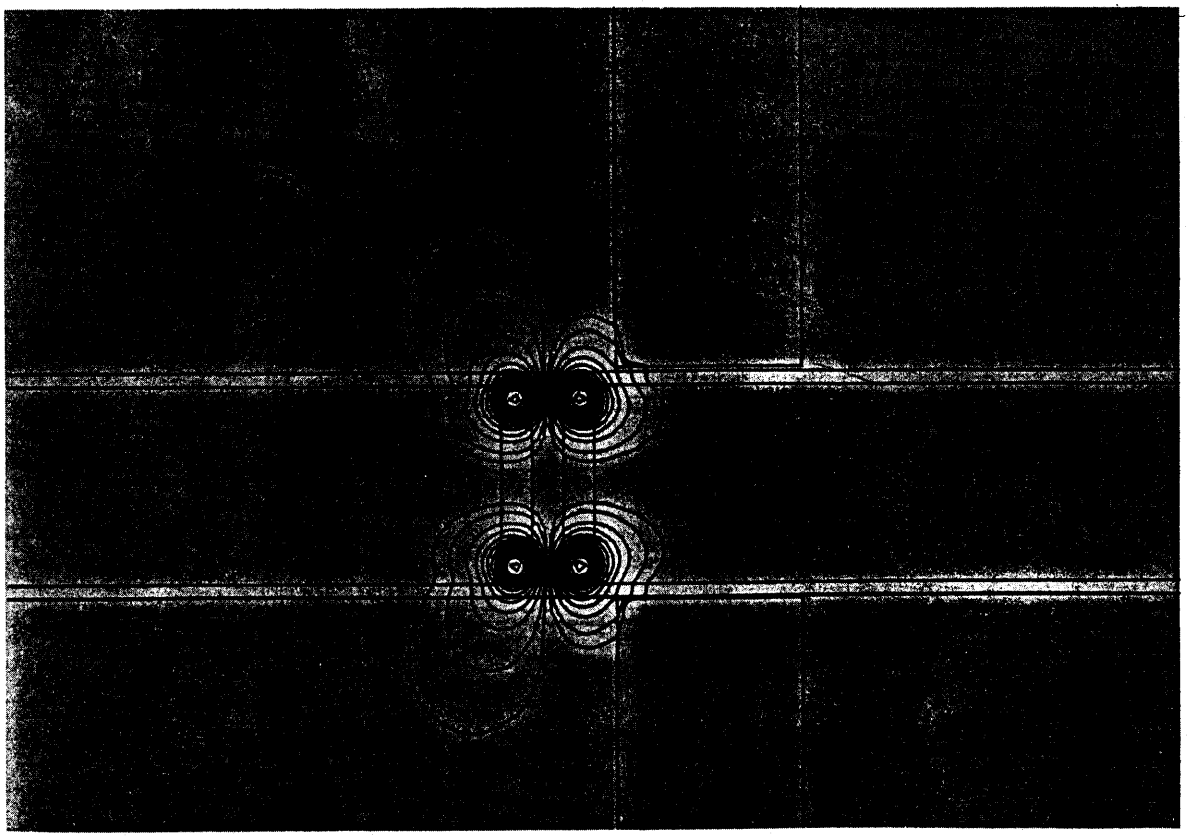

Figure 6. Contour plot showing the leading coil affected by the edge of the support plate.

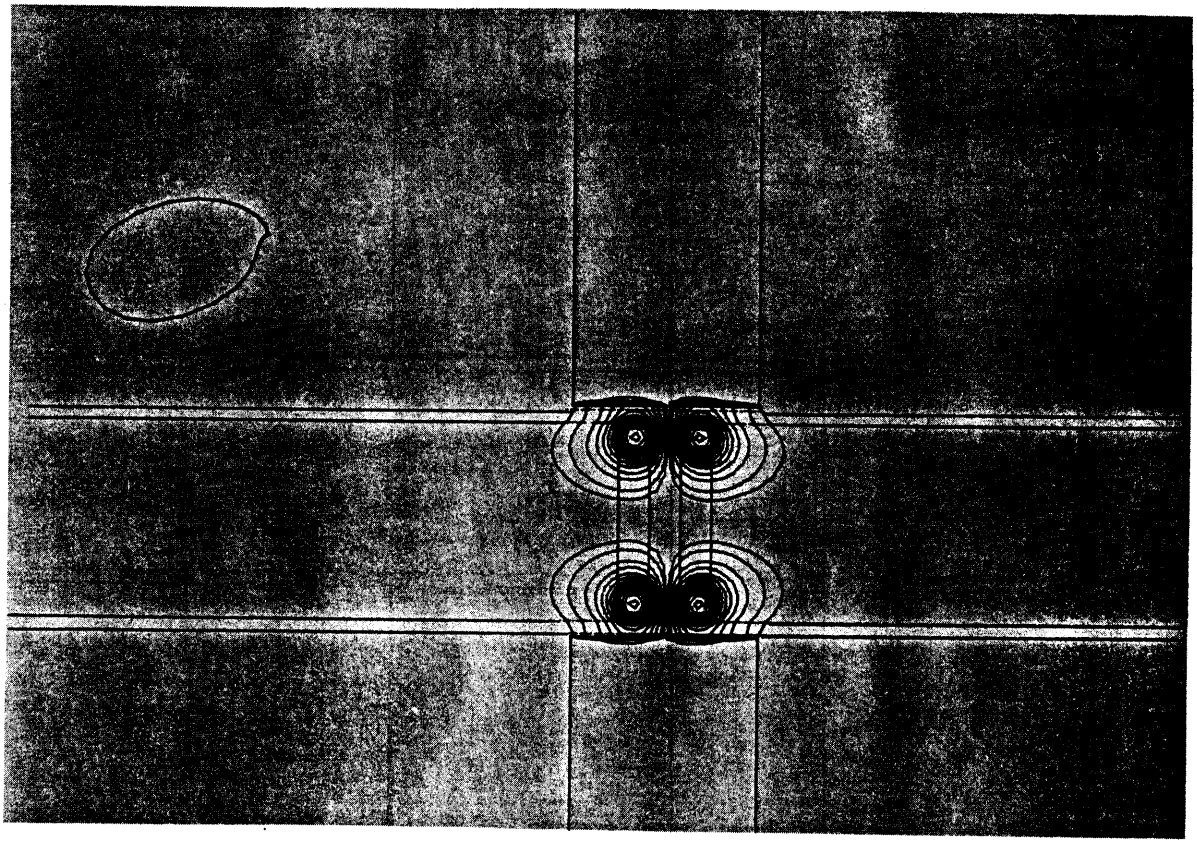

Figure 7. Contour plot showing the coil centered in the support plate (half of the impedance plane trajectory is complete).

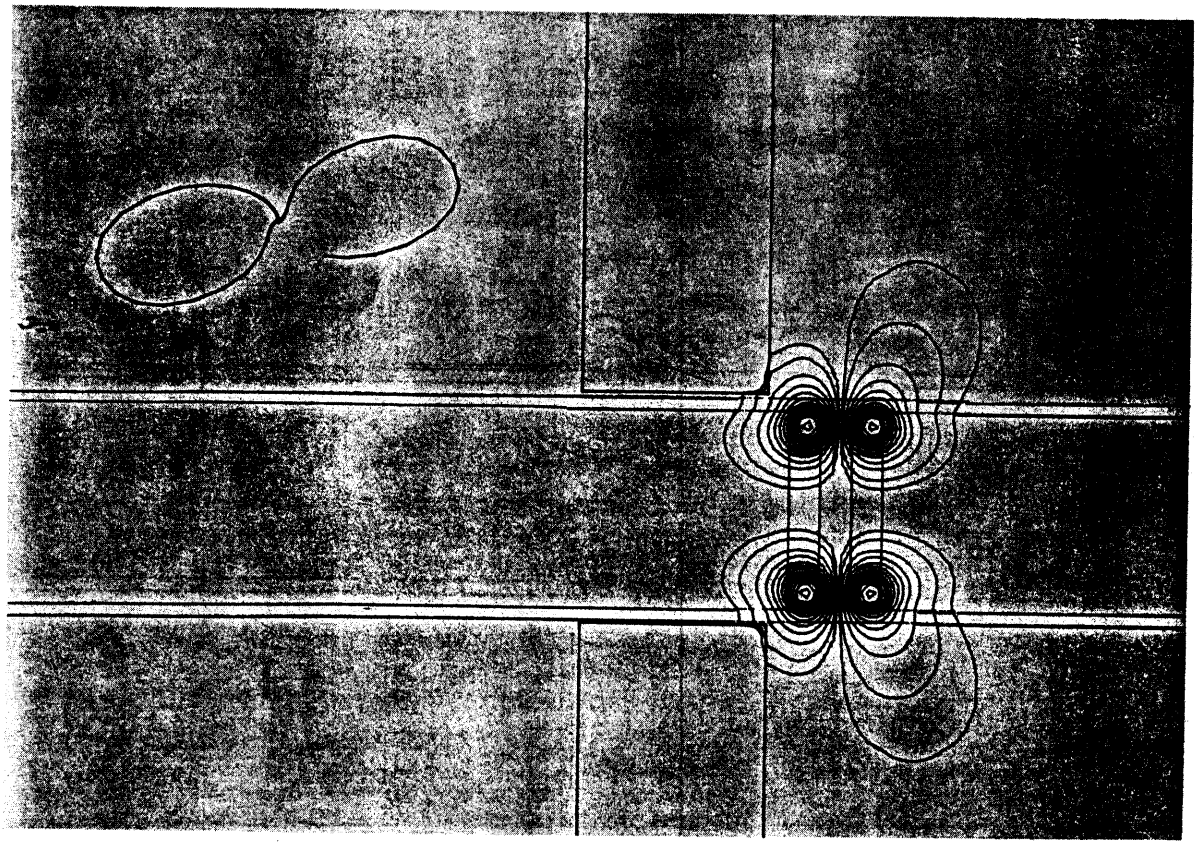

Figure 8. Contour plot showing the trailing coil leaving the support plate region.

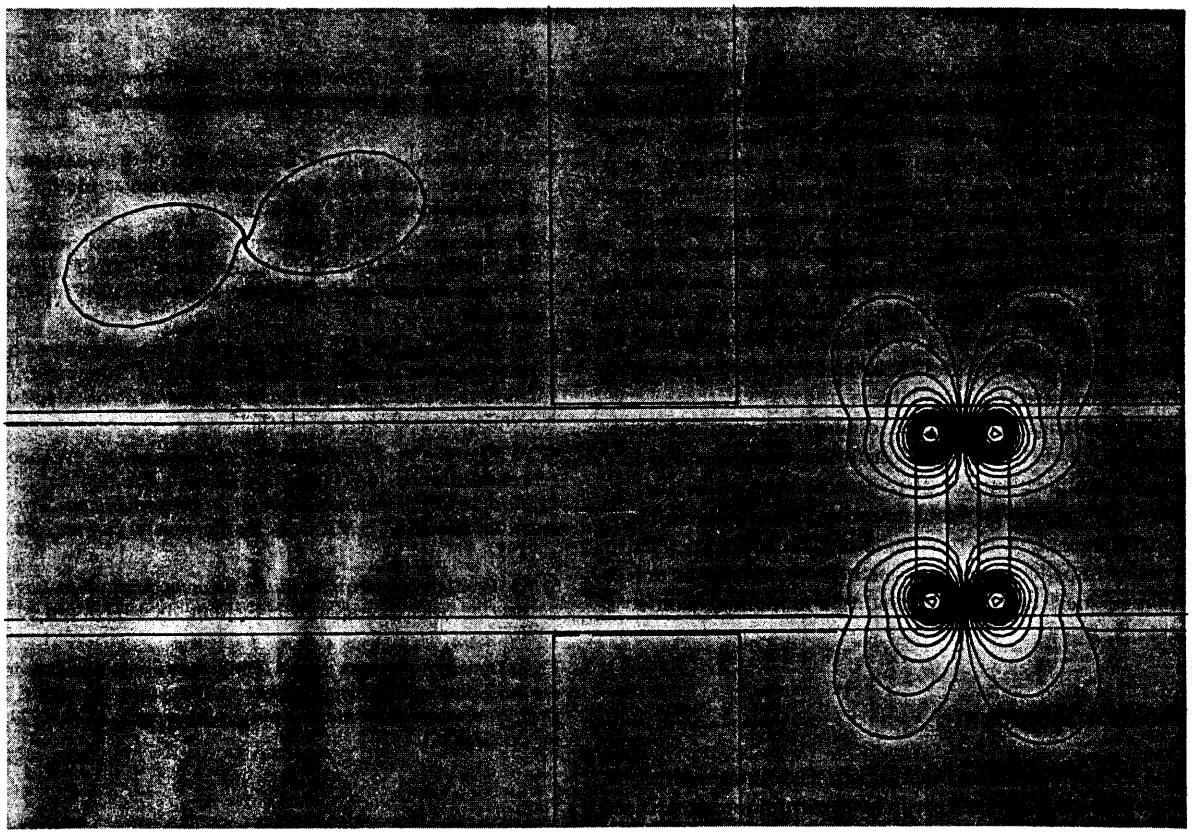

Figure 9. Contour plot showing the coils outside the support plate region (the impedance plane trajectory is complete).

Figures 8 and 9 are reflections of Figures 6 and 5, respectively, but the change in coil impedance is due to the other coil in the probe; this then describes another loop that is identical to the previous one since all the conditions remain the same.

The changes in the flux distribution and in the impedance trajectory are quite fast when the coils approach the support plate or depart from it, but there is little or no change when they are well away from or inside the support plate. The flux distribution seems, in fact, to "collapse" as the probe approaches the support and then to reopen again when it leaves. This phenomenon is also noticed when measurements are taken in real testing of steam generator support plates. An additional property that these plots demonstrate is that the penetration of the field inside the support plate is small due to its high permeability.

To complement the animation sequence, we designed and built a mock-up of the support plate and tube. The mock-up was constructed using a piece of Inconel tubing and a portion of ¾-inch carbon steel support plate. A cut was made through the support plate and tube to reveal the coil movement, shown in Figure 10. The probe's coils, which are about 0.080-inch wide and about the same distance apart, are clearly visible in the figure. The loop in Figure 11 is a photograph of an eddy current oscilloscope screen, showing the impedance trajectory for a support plate surrounding an Inconel tube as the probe moves past the support plate.

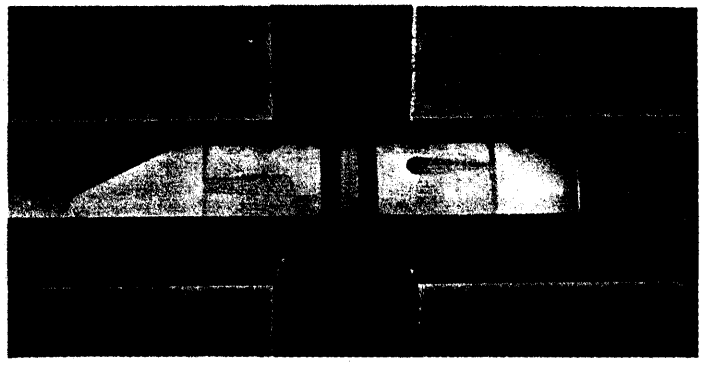

Figure 10. Mock-up of the support plate and Inconel tube with a differential eddy current probe inside the tube.

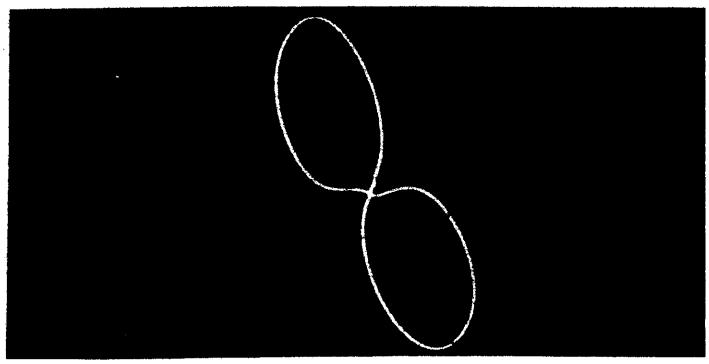

Figure 11. Impedance plane trajectory of a carbon steel support plate taken with an NDT-15 Eddyscope.

Concluding remarks

Numerical techniques such as finite element analysis are solving many engineering problems previously deemed unsolvable with analytical approaches. The NDT example illustrated in this article is typical of a whole class of energy/material interactions that have traditionally been difficult to model either analytically or experimentally. Combining powerful numerical techniques with computer graphics capabilities shows some promise not only of providing useful insight into the physics of NDT, but also of aiding in the design of probes and yielding clues to the solution of the inverse or defect characterization problem.

Indeed, the use of a graphics and/or film capability is imperative in this type of problem—a problem where large, complex numerical programs have to be run repeatedly in order to simulate probe motion. We are now extending our work to three-dimensional geometries to predict impedance plane trajectories from realistic defect shapes such as pits, corrosion, and nonaxisymmetric cracks. ■

Acknowledgment

The work described in this article was supported by the Electric Power Research Institute under project RP1395-2.

References

1. H. L. Libby, *Introduction to Electromagnetic Nondestructive Test Methods,* Wiley-Interscience, New York, 1971.
2. A. M. Winslow, "Numerical Solution of the Quasilinear Poisson Equation in a Nonuniform Triangle Mesh," *J. Computational Physics,* Vol. 2, 1967.
3. P. Silvester and M. V. K. Chari, "Finite Element Solution of Saturable Magnetic Field Problems," *IEEE Trans. Power Apparatus and Systems,* Vol. 80, 1970, pp. 1642-1651.
4. J. H. Hwang and W. Lord, "Finite Element Analysis of the Magnetic Field Distribution Inside a Rotating Ferromagnetic Bar," *IEEE Trans. Magnetics,* Vol. Mag-10, No. 4, Dec. 1974, pp. 1113-1118.
5. W. Lord and R. Palanisamy, "Development of Theoretical Models for NDT Eddy Current Phenomena," in *Eddy Current Characterization of Materials and Structures,* ASTM STP 722, G. B. Birnbaum and G. Free, eds., 1981.
6. O. C. Zienkjewicz, *The Finite Element Method in Engineering Science,* McGraw-Hill, London, 1971, third ed., 1976.
7. J. Donea, S. Givliani, and A. Phillipe, "Finite Elements in the Solution of Electromagnetic Induction Problems," *Int'l J. Numerical Methods in Engineering,* Vol. 8, 1974, pp. 359-367.

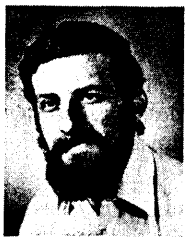

Nathan Ida is a research assistant professor with the electrical engineering department at Colorado State University, Fort Collins, Colorado. From 1979 to 1983 he worked as a graduate research assistant at the university. His research interests include numerical analysis, modeling electromagnetic fields, and nondestructive testing phenomena.

Ida received his BSc and MSc in electrical engineering from the Ben-Gurion University, Beer Sheba, Israel, and his PhD from Colorado State University. He is a member of the IEEE.

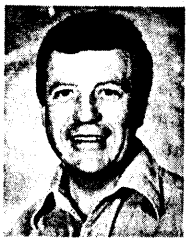

William Lord is a professor of electrical engineering at Colorado State University. His industrial research experience includes consulting work with the Systems Development Division of IBM, the Inland Motor Division of Kollmorgen Corporation, Exxon Research, and Schlumberger. He has also taught electrical engineering at the University of Tennessee and Clarkson College of Technology. Lord's current research interests relate to the use of numerical analysis techniques for modeling field/defect interactions associated with electromagnetic methods of nondestructive testing.

Lord received a PhD in electrical engineering from Nottingham University, UK, in 1964. He is a chartered engineer and fellow of the IEE, a senior member of the IEEE, and is also a member of the American Society for Engineering Education, the American Society for Nondestructive Testing, Sigma Xi, and Eta Kappa Nu.

IEEE Computer Graphics and applications

May/June 1983 Volume 3 Number 3 (ISSN 0272-1716)

ARTICLES

Cover: "Twin-Headed Mythological Lizard Woman," computer graphics art by Mowgli, aided by the Lactamme laboratory. See "About the Cover" on page 6.

Cover design: Russ Ono

DEPARTMENTS

Coming in July:
Computerized Slide-Making

Coming in August:
Computer Graphics in Medicine and Biology

Published by the IEEE Computer Society
in cooperation with
the National Computer Graphics Association

IEEE CS Membership Application, p. 57
Reader Service Cards, p. 97
Order Form, p. 97

IEEE
Computer Graphics
plications

5

Solid Modeling fo
Mechanism Desig

Simulatin
Nondestructiv
Testin

MAY/JUNE 1